REGULAR PAPER

Differential optical absorption spectroscopy-based refractive index sensor for cancer cell detection

Tarunnum Parvin[1] · Kawsar Ahmed[2] · Aadel M. Alatwi[3] · Ahmed Nabih Zaki Rashed[4]

Abstract

A novel spectroscopic optical sensor is presented for cancerous cell detection in various parts of the human body (i.e., cervix, adrenal gland, breast, skin, and blood). An optimized structure based on compact cladding is successfully designed with enhanced sensitivity and very low confinement loss. The parameters like effective area (A_{eff}), V-parameter (V_{eff}), spot size (W_{eff}), numerical aperture (NA), and beam quality factor are investigated over the wavelength region 1.4–2.5 μm. The consummation of relative sensitivity is also calculated and is superior to other previous work. The numerical investigation indicates that cancerous cells have higher sensitivity than normal cells. The values investigated for the sensitivity of cervical cancer, adrenal gland cancer, skin cancer, blood cancer, and breast cancer of type I and type II are 94.96%, 95.15%, 94.13%, 94.84%, 95.40%, and 95.51% in X-polarization, respectively, which are higher than the calculated values from any prior works. The explored structure is monomode PCF, with silica as a dielectric material. The finite element method (FEM) has been implemented for investigating the numerical values, implemented on COMSOL Multiphysics (version 5.3). The simple design ensures easy fabrication with ongoing techniques.

Keywords Optical sensor · Sensitivity · Cancer cell sensing · Loss profile · Spot size · Beam quality factor

1 Introduction

Due to its great potential in sensing applications, photonic crystal fiber (PCF) has been the most in-demand technology for enhancing the performance and minimizing the fabrication cost of various categories of optical fiber for the last 30 years. PCF is a revolutionary new class of fiber, packed with much flexibility in its design. It is a low-loss microstructure fiber that uses photonic crystal material for its core and cladding. By altering the size, shape, and arrangement of air holes, the optical and guiding properties can be enhanced. PCF is used in many applications, such as nonlinear devices, fiber lasers, and biosensors that are used in chemical industries for the detection, prevention, and treatment of various kinds of diseases. In PCF, light is propagated either by the photonic bandgap or by total internal reflection.

Numerous applications of PCF in biosensing make PCF of great interest in implementing various types of sensors. PCF is currently an auspicious technology for sensing applications due to its powerful light–matter interaction. In comparison to photonic bandgap, the index-guided PCF is more appropriate for sensing liquids. Due to various real-life

✉ Kawsar Ahmed
  kawsar.ict@mbstu.ac.bd; k.ahmed.bd@ieee.org;
  kawsarit08050@gmail.com

  Tarunnum Parvin
  tarannumparveen09@gmail.com

  Aadel M. Alatwi
  aadel.alatwi@ut.edu.sa

  Ahmed Nabih Zaki Rashed
  ahmed_733@yahoo.com

1 Deparment of Electronics and Communication Engineering, Birla Institute of Technology (B.I.T) Mesra (Patna Campus), Bihar 800014, India

2 Department of Information and Communication Technology (ICT), Group of Biophotomatix, Mawlana Bhashani Science and Technology University (MBSTU), Tangail 1902, Bangladesh

3 Electrical Engineering Department, Faculty of Engineering, University of Tabuk, Tabuk, Saudi Arabia

4 Electronics and Electrical Communications Engineering Department, Faculty of Electronic Engineering, Menoufia University, Menouf 32951, Egypt

applications, SPR-based sensors are popular items of interest for researchers. It is highly applicable to chemical sensing, blood component detection, various types of disease detection, harmful additive detection, and more [1–4]. Due to advancements in photonic technology, the implementation of sensors with rapid detection, enhanced sensitivity, and low confinement loss is now possible. Spectroscopic sensors have already proved their potential in various fields, such as disease detection, chemical sensing of toxic materials, and more [5, 6]. Although various spectroscopy-based sensors have been implemented for disease detection, the detection of cancer cells with very high sensitivity and low confinement loss is introduced in this article. The cancerous cells are categorized as stage-I, stage-II, and stage-III. In stage-I, patients can be cured. In Stage-II, patients may also be cured but patients naturally cannot be cured in stage-III. It is necessary to detect cancerous cells at an early stage for better treatment. Many techniques, such as electrochemical methods and artificial intelligence, have introduced for detecting cancerous cells in the cervix, breast, and different parts of the body. However, these methods are comparatively very complex. A requirement of cancer-testing equipment is the ability to detect the cancerous cell in a short time. For the detection of cancer, we consider blood and other fluid substances from the affected parts of a human body, which directly measure the refractive index of cancer cells. In 2014, Sharan et al. proposed the detection of cancer cells by using the photonic bandgap method [9]. However, the photonic band gap method experiences difficulty in the fabrication process. Additionally, the thermal profile has an impact on the outcome. In the following year, Sharma et al. proposed a 2D photonic crystal sensor for the investigation of cancerous cells in basal, breast, and cervical cases [8]. The operating wavelength range was very small. In addition, the fabrication tolerance was not introduced. In 2018, Ramanujan et al. proposed a dimensional coated nanocomposite material based photonic crystal for detecting cancerous cells [7]. They applied the surface plasmon resonance (SPR) technique for sensing and gained very low sensitivity. In the middle of 2018, Shimohammadli et al. designed a microfluidic device for breast cancer screening [10]. In the same year, Ayynar et al. proposed a dual-core PCF sensor for detecting cervical, breast, and basal cancers [5]. Although they reported the improved sensitivity performance, the detection limit was very low. In 2019, Jabin et al. presented a cancer sensor that is based on SPR for the fast detection of various types of cancerous cell with the improvement of sensitivity response and detection limit [2]. Moreover, a new amoeba-shaped structure was designed and more optical parameters are also analyzed but the relative sensitivity response was not so good though the other parameters response was good [11]. As a result to overcome these limitation or to increase the sensitivity percent the proposed investigation is

performed. Additionally, to the best of our knowledge, differential optical absorption spectroscopy-based cancer cell detection sensor has not been proposed yet. So, there is still room to design such a refractive index-based optical sensor.

In this study, a spectroscopy-based compact cladding PCF is introduced. Simplification in design with optimized sensitivity and low confinement loss provides easier fabrication with better results for the detection of several cancerous cells: blood cancer, cervical cancer, gland cancer, breast cancer of type-I and type-II, and skin cancer. A large number of parameters are analyzed in this proposed work such as guiding properties, sensitivity response, loss value, effective area, V-parameter, Sport size, beam divergence, and numerical aperture. The maximum sensitivity response with low loss value is gained from the suggested work. So, it is estimated that the modified sensor will be implemented for further investigations.
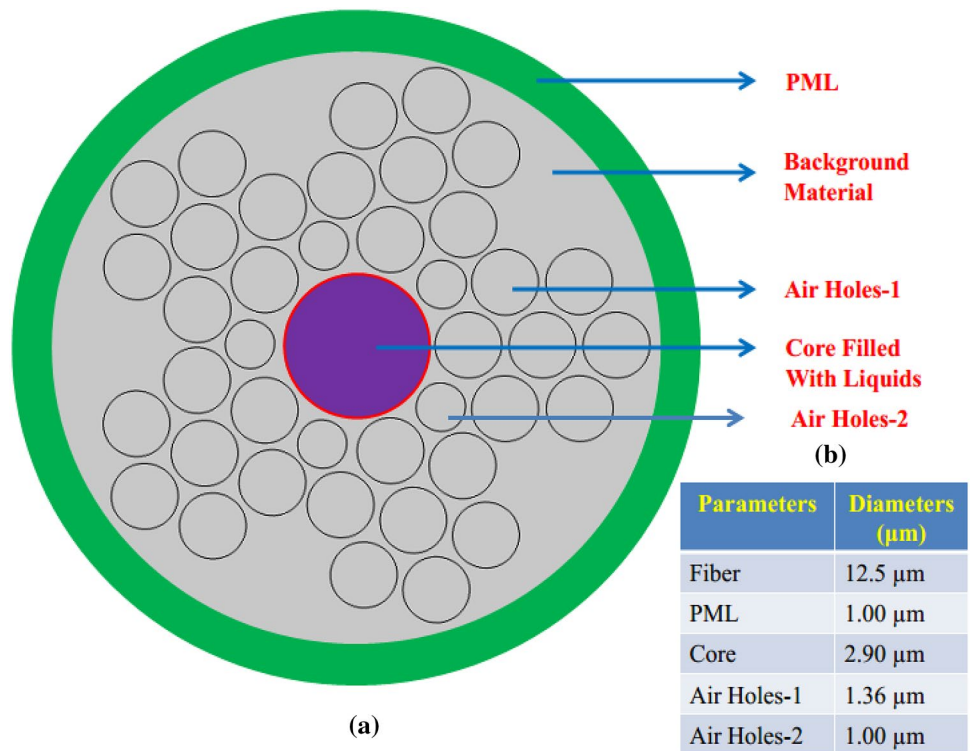
2 Design methodology of cancer sensor

The proposed PCF is made of compact cladding using a circular lattice of air holes. This PCF is proposed as a cancer sensor for the detection of various types of cancer cells. The core region is surrounded by a compact cladding containing circular air-holes. In the cladding part, each circular air hole is surrounded by six air holes. The diameter of the core is 2.9 μm, while the air filling factor for the inner core circle is 1.9 μm. These values of the structural design parameters are gained from tuning the values. It is noticed that the core diameter as well as the air hole shape and size highly affect the light propagation mode. In Fig. 1b, the description of each parameter is described with the value of diameters. Simplicity in design makes the proposed sensor easy to fabricate using the latest techniques (e.g., sol–gel, extrusion). The wavelength operating range makes the proposed cancer sensor significant and auspicious. The proposed structure is constructed using the COMSOL Multiphysics software (version 5.3). Its optical behavior is analyzed by the full vector finite element method (FV-FEM). The accuracy of this method is high than other well-known numerical approaches. Because this method splits the model into large numbers of mesh elements like 45,324. Due to the fixed number of degree freedom FEM is best suited for electromagnetic probe. A simple design is proposed here to reduce complexity and manufacturing cost.

3 Cancer sensor guiding properties

Figure 1a shows the proposed structure of a spectroscopy-based cancer sensor for the fast detection of various types of cancer cells, such as adrenal gland cancer (PC12), blood

Fig. 1 Cross sectional view of the proposed cancer sensor

(a)

Parameters	Diameters (μm)
Fiber	12.5 μm
PML	1.00 μm
Core	2.90 μm
Air Holes-1	1.36 μm
Air Holes-2	1.00 μm

(b)

cancer (Jurkat), breast cancer (MDA-MB-231 and MCF-7), cervical cancer (HeLa), and skin cancer (basal). In this article, a better performance for the fast detection of cancer from cell fluid (80% of concentration) relative to its normal cell (30–70% of concentration) is achieved. The outcomes of the index of refraction of normal cells and cancer cells are quite different. Normally, cancer cell size variation depends upon the types of cancer cells. The cervical cancerous cell size is 17.66 μm, the breast cancer cell size is 17.48 or 18.72 μm, and the basal cancer cell size is 30 μm [5]. Silica is taken as the background material. The simulation is done using Sellmeier's equation [12].

$$n^2 - 1 = \sum_{x=1}^{3} \frac{A_x \lambda^2}{\lambda^2 - B_x^2}. \qquad (1)$$

In expression (1), n is the index of refraction for specified wavelength λ (μm), A_x and B_x are the constants parameters that have fixed values and are taken from [12]. Here A_1, A_2, and A_3 values are 0.69616630, 0.40794260, and 0.89747940, respectively, and B_1, B_2, and B_3 values are 0.06840430, 0.11624140, and 9.8961610, respectively. Table 1 lists the refractive index of normal and cancer cells according to the concentration level. Table 1 represents the refractive indices lists of different cancer cells that are used in this investigation. Here, the cancer cell variations and concentrations mixers are highlighted. In addition, (MDA)-(MB)-231 is known as Type-I and MCF-7 is known as Type-II for breast cancer.

In figure legends, breast cancer Type-I and Type-II are conducted for cell (MDA)-(MB)-231 and MCF-7 respectively.

3.1 Sensitivity

The amount of light interacted with analytes is depicted by relative sensitivity and is evaluated by [13]:

$$R_S = \frac{n_c}{\text{Re}[n_{ei}]} \times F_p. \qquad (2)$$

In expression (2), n_c is the index of refraction of the cancerous cell, n_{ei} is the effective index of refraction at that precise wavelength, R_S is the coefficient of relative sensitivity, and F_P is the ratio (%) of the core power and overall power.

Using the pointing theorem, the fraction of core power can be calculated [13]:

$$F_p = \frac{\int_{\text{Core}} \text{Re}\left(E_x H_y - E_y H_x\right) \, \mathrm{d}x\mathrm{d}y}{\int_{\text{Overall}} \text{Re}\left(E_x H_y - E_y H_x\right) \, \mathrm{d}x\mathrm{d}y}. \qquad (3)$$

In expression (3), E_x and E_y are the electric fields and H_x and H_y are the magnetic fields. The numerator of the above expression is accomplished for the cancer cells sensed in the core area and the denominator is taken as the overall region of the fiber. Figure 2 represents the mode filed distributions of the highlighted cancer sensor in both polarizations and ensures tight confinement of light through the core area. So,

Table 1 Refractive index of different cancer cells as well as normal cells according to concentration level

Name_Cell	Types of cell and its concentration level (%)	Refractive_Index	References
Jurkat	Blood_Cancer (80%)	1.390	[2, 8, 17, 18]
	Normal_Cell (30–70%)	1.376	[2, 8, 17, 18]
HeLa	Cervical_Cancer (80%)	1.392	[2, 8, 17, 18]
	Normal_Cell (30–70%)	1.368	[2, 8, 17, 18]
PC-12	Adernal Gland_Cancer (80%)	1.395	[2, 8, 17, 18]
	Normal_Cell (30–70%)	1.381	[2, 8, 17, 18]
(MDA)-(MB)-231	Breast_Cancer (80%)	1.399	[2, 8, 17, 18]
	Normal_Cell (30–70%)	1.385	[2, 8, 17, 18]
MCF-7	Breast_Cancer (80%)	1.401	[2, 8, 17, 18]
	Normal_Cell (30–70%)	1.387	[2, 8, 17, 18]
Basal	Skin_Cancer (80%)	1.380	[2, 8, 17, 18]
	Normal_Cell (30–70%)	1.360	[2, 8, 17, 18]

Fig. 2 Light confinement outline of the PCF; **a** X-polarization and **b** Y-polarization
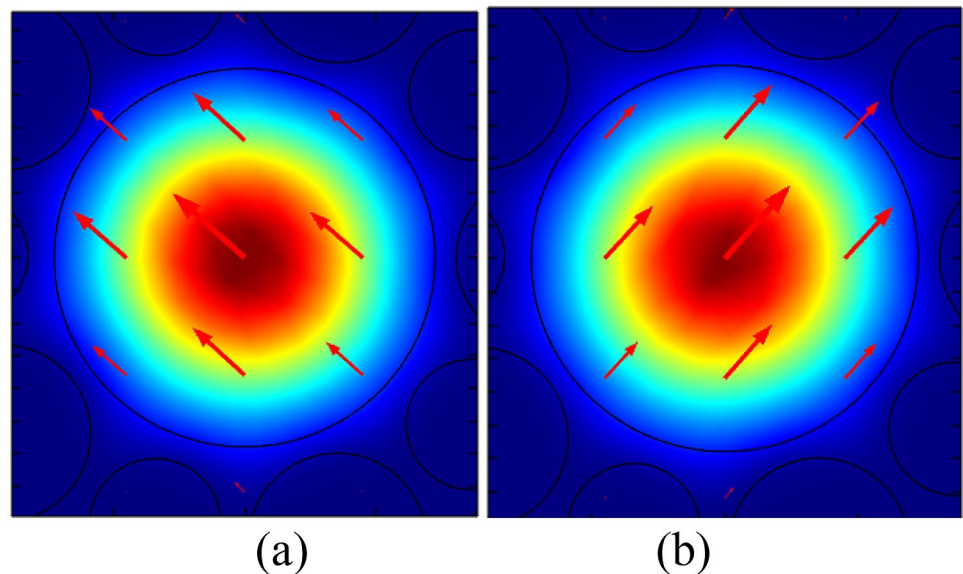
both the power fraction and the sensitivity response will be high.

Figure 3 shows the relative sensitivity of the various cancerous cells with respect to wavelength in the X and Y-polarization modes based on the Eq. (2). Comparing the sensitivity of cancerous cells with that of the normal cell, the sensitivity of the cancerous cell is more than that of the normal cell. The higher refractive index cancerous cell has more sensitivity. The above graph shows that the breast cancer cell of refractive index 1.401 has higher relative sensitivity. Also, the higher wavelength sensor shows higher sensitivity for the corresponding cancerous cell. The highest relative sensitivity is observed at 2.5 µm. Light interacts more strongly at a higher wavelength. Keeping the parameters the same, the proposed sensor relative sensitivity is calculated for Y-polarization mode. No more changes in Y polarization are observed, the same as X polarization higher relative

sensitivity is observed at a higher wavelength. For the entire cancerous cell sensitivity, up to 90% is observed for the higher value of wavelength. It was determined that the interaction of light with cancerous cells gives better results at higher wavelengths both in X and Y polarizations. The relative sensitivity is obtained for X-polarization of 94.96%, 95.15%, 94.13%, 94.84%, 95.40%, and 95.51% for cervical cancer, adrenal gland cancer, skin cancer, blood cancer, and breast cancer of type I and type II, respectively. The sensitivity investigated for Y polarization is 94.83% for blood cancer, 94.96% for cervical cancer, 95.39% for breast cancer of type-I, 95.51% for breast cancer of type-II, 94.14% for skin cancer, and 95.15% for gland cancer. The comparison chart for the sensitivity response analysis with prior works is given in Table 2.

From Table 2, it can be claimed that the maximum sensitivity response gained from the proposed work is the highest
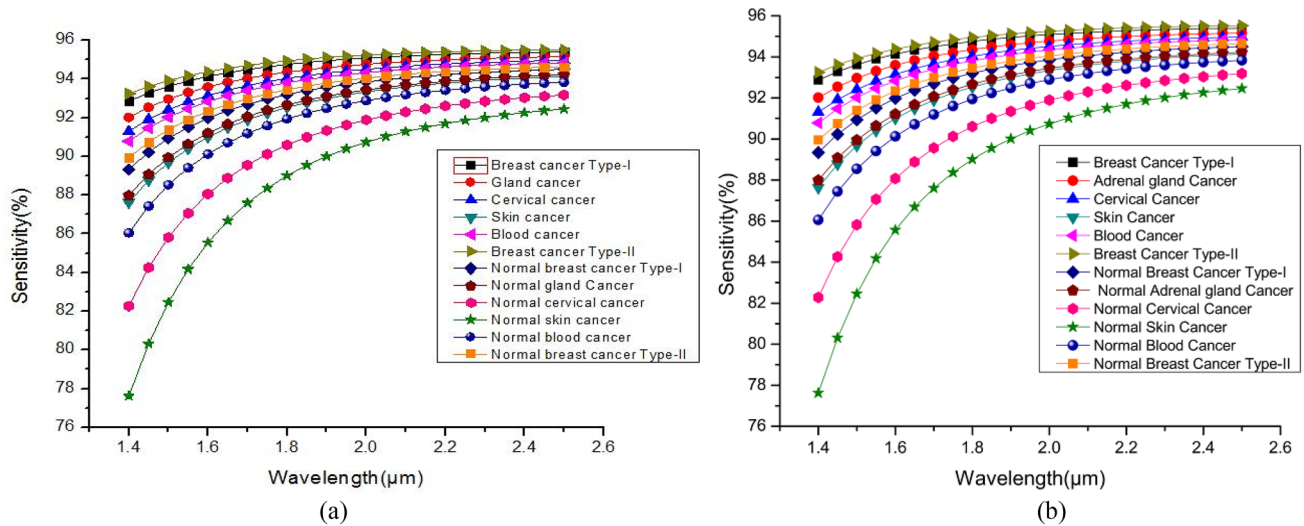
Fig. 3 The sensitivity Vs wavelength for the proposed design in **a** *X*-polarization and **b** *Y*-polarization

Table 2 The comparison of sensitivity response with respect to the prior articles

Sensor structure	Maximum sensitivity response (%)	References
Quasi PCF	72.19	[14]
PCF	55.56	[15]
Kagome PCF	85.7	[3]
PCF	95.51	Proposed work

than the previously analyzed responses. So, it can be estimated that the calculated results for both types of polarizations (i.e., *X* and *Y*) are higher than the values calculated in any prior works.

3.2 Confinement loss

Confinement loss is an important parameter for sensors. The assimilation is done by taking the imaginary part of the effective refractive index. Light penetrates from the core to the cladding region due to the finite number of air holes. Due to tight confinement of light, very low confinement loss is observed both in X and Y polarization according to expression (4) [16].

$$L_c = \frac{40\pi \cdot \mathrm{Im}(n_{\mathrm{eff.}}) \cdot 10^6}{\lambda \cdot \ln(10)} \, \mathrm{dB/m}. \tag{4}$$

Here, L_c specifies the confinement loss and $\mathrm{Im}(n_{\mathrm{eff.}})$ represents the imaginary part of the effective refractive index. From Fig. 4, it is seen that the confinement loss is very low (lowest scale of 10^{-9}) up to 2.2 µm. After that,

the confinement loss increases with respect to wavelength. The increment of loss is very low (highest scale of 10^{-4}) for the investigated range of all analytes. The outcomes are highly comparable with prior studies. In addition, the differences between the confinement losses of *X*-polarization (in Fig. 4a) and *Y*-polarization (in Fig. 4b) are very close to each other. As the light intensity changes for the two polarizations so the confinement losses are also changed. But these changes are very small.

3.3 Effective area

The area surrounded by the mode fields in the core section is evaluated by an effective area (A_{eff}). The A_{eff} of a PCF can be evaluated by the following expression (5) [16].

$$A_{\mathrm{eff}} = \frac{\left[\int I(r.)r.\mathrm{d}r.\right]^2}{\left[\int I^2(r.)r.\mathrm{d}r.\right]^2} \tag{5}$$

In expression (5), $I(r.) = |Et|^2$ represents the amount of transverse electric field.

The light intensity variations are the main reason for changing the effective area. The light intensity that propagates through the core changes for the polarized modes. That means different light intensity propagates for the *X* and *Y* polarizations. For this reason, the effective area is also changed. In Fig. 5, it is demonstrated that A_{eff} trends upward with an increase in wavelength for both types of polarization. At lower wavelengths, light pulses are more confined in the core region. It is observed that as A_{eff} increases, the relative sensitivity also increases for a higher
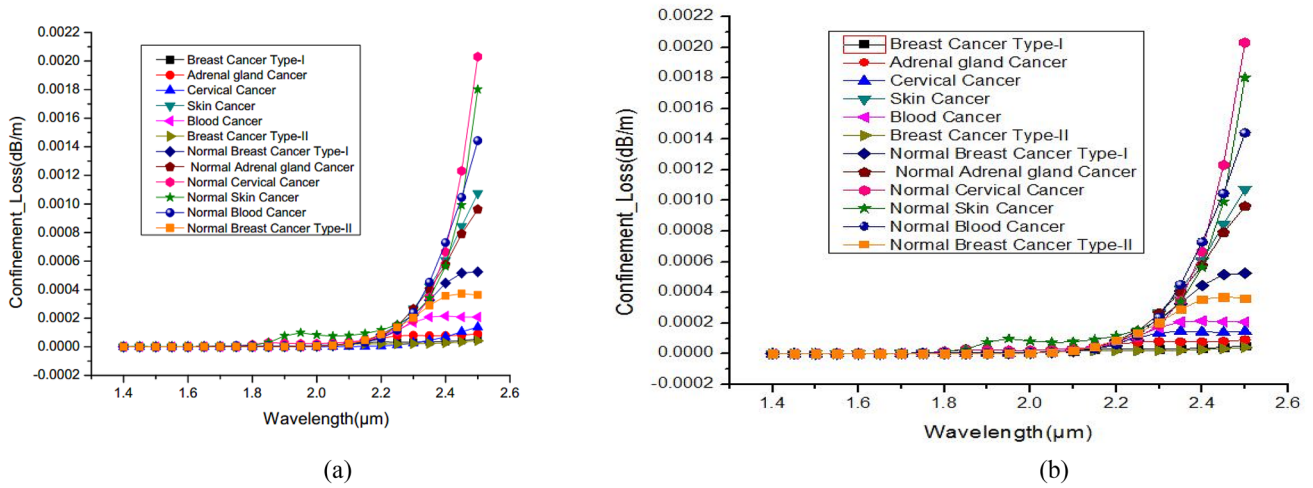
Fig.4 Confinement loss vs wavelength for the proposed structure in **a** X-polarization and **b** y-Polarization
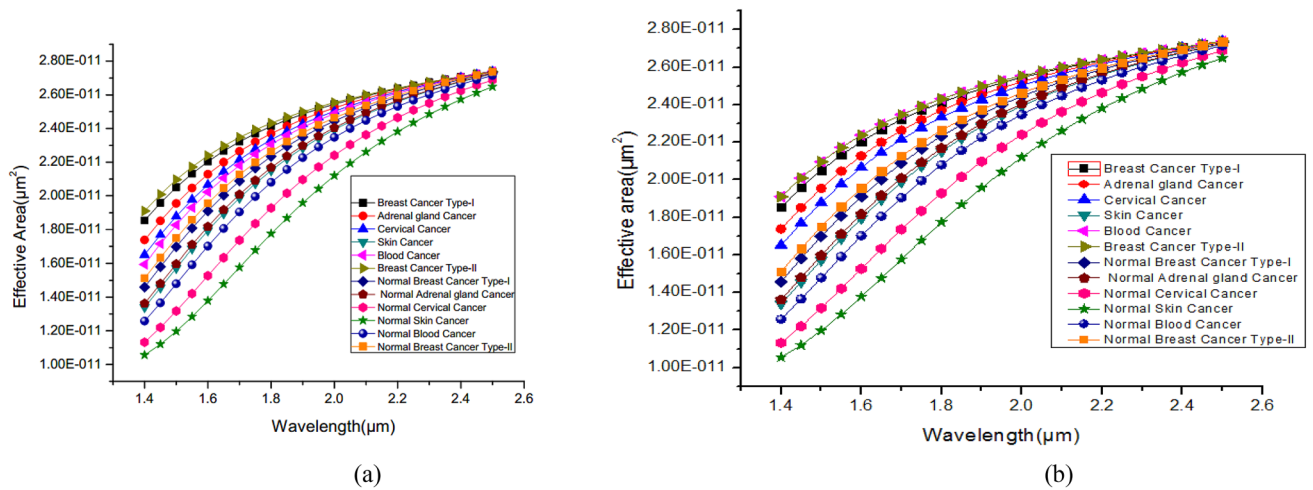

Fig. 5 The effective area vs wavelength for the suggested structure in **a** X-polarization and **b** Y-polarization

degree of modal diffusion due to more light-to-cancer-cell interaction. This enhances its sensing characteristics.

3.4 V-parameter

The normalized frequency or V-Parameter (V) of a PCF is stated by expression (6), where values less than 2.405 ($V < 2.405$) indicate a mono-mode waveguide and values more than 2.405 ($V > 2.405$) indicate a multimode waveguide [17].

$$V = \frac{2\pi R}{\lambda}\sqrt{n_{co}^2 - n_{cl}^2}. \tag{6}$$

Here, n_{co} is the refractive index of the core region and n_{cl} is the index of refraction of the cladding region.

In Fig. 6, as wavelength increases, the value of V_{eff} decreases for both X and Y polarization. Its highest values are 2.0151 for breast cancer for both types of polarization at 1.4 μm, which is less than 2.405; hence, the proposed structure is monomode. The monomode behavior helps the proposed sensor for long-distance sensing applications and makes the sensor a prominent candidate in the area of sensing.

3.5 Spot size

Spot size and beam divergence are two essential parameters for all biosensors. The relationship between spot size and V can be analyzed by the Marcuse formula, given in expression (7) [18]. The modal spot size W_{eff} can be evaluated as:
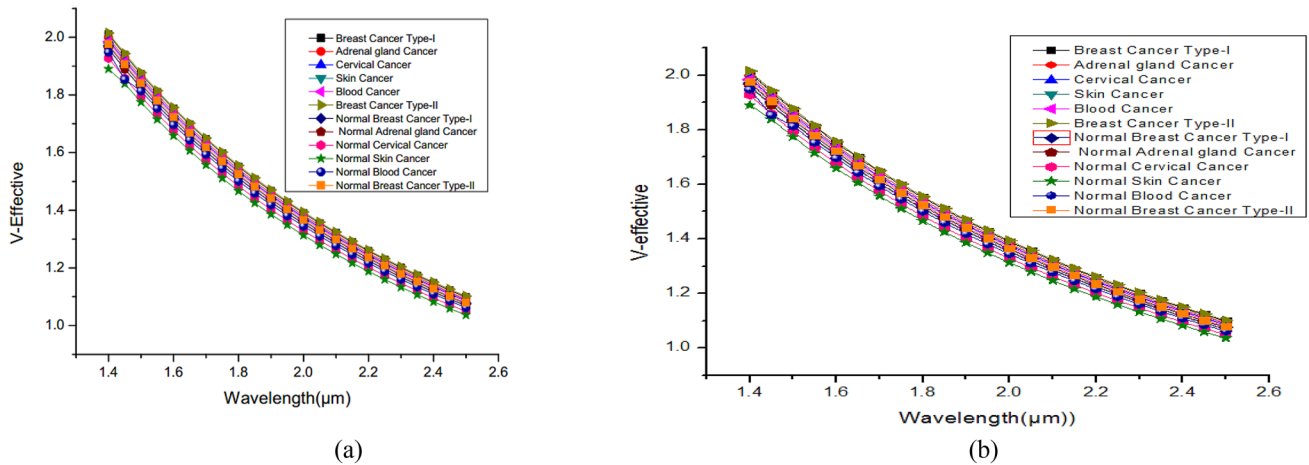
Fig. 6 The V-effective vs wavelength for the suggested design in **a** X-polarization and **b** Y-polarization

$$W_{\text{eff}} = R \times \left(0.65 + \frac{1.619}{V^{\frac{3}{2}}} + \frac{2.879}{V^6} \right). \qquad (7)$$

Here, R is defined as the core radius and V is the normalized frequency. As shown by Fig. 7, the higher refractive index cancer cells (i.e., breast cancer cells of type-II) have lower spot sizes. Also, at higher wavelength, the spot size increases. In Fig. 7, it is demonstrated that the spot size increases with wavelength. This is a favorable sign for a sensor because the increment of spot size enhances the beam-focusing quality.

3.6 Beam divergence

The light beam quality is measured by the beam divergence when it is passed through a fiber. Beam divergence of the PCF can be evaluated from Gaussian-beam theory using the following expression [19].

$$\theta = \tan^{-1} \left(\frac{\lambda}{\pi W_{\text{eff}}} \right). \qquad (8)$$

Here, θ represents the beam divergence angle and is measured in radians, λ represents the operating wavelength, and W_{eff} is the spot size. Larger beam divergence specifies poor beam converging or beam quality. In Fig. 8, it is illustrated that the beam divergence is increasing with increasing wavelength.
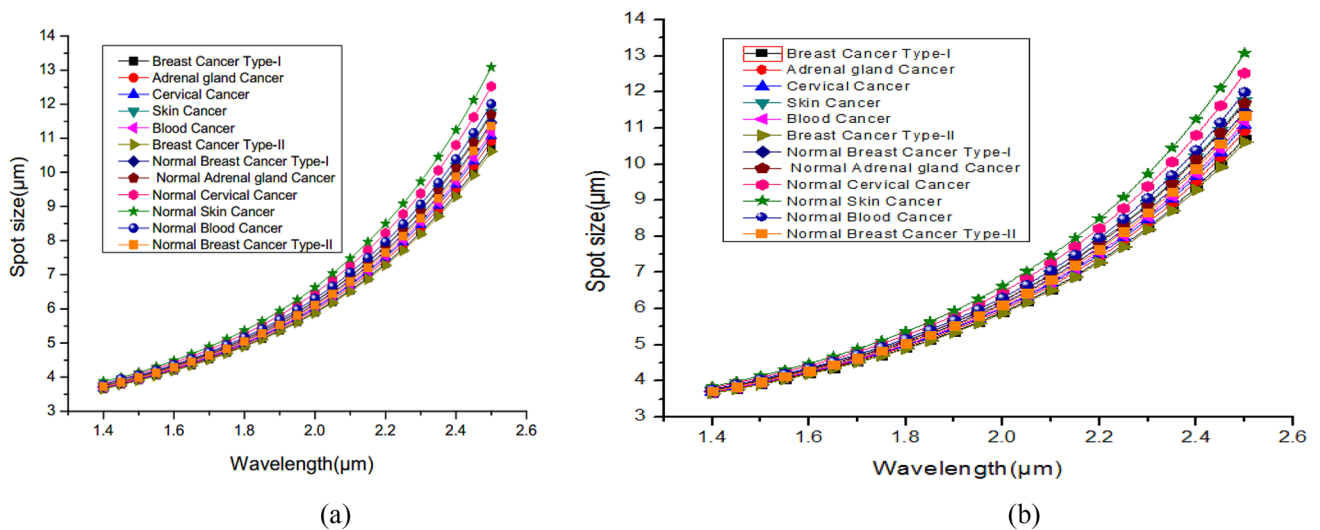

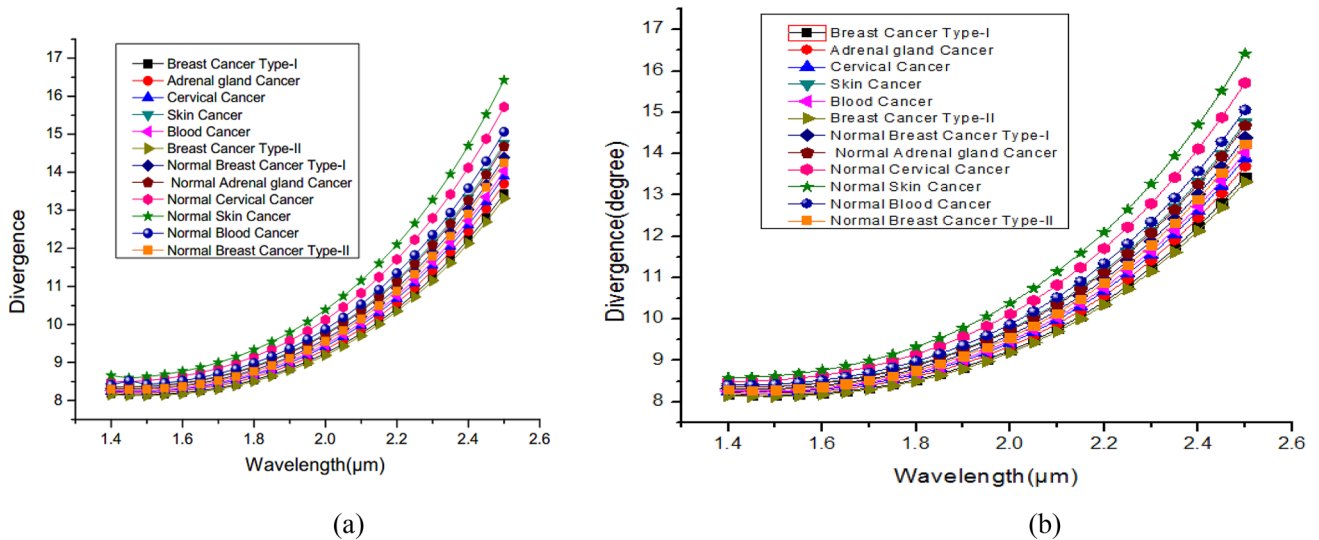Fig.7 The spot size vs wavelength for the suggested design in **a** X-polarization and **b** Y-polarization

Fig. 8 Divergence vs wavelength for the suggested structure in **a** *X*-polarization and **b** *Y*-polarization

This phenomenon indicates inferior beam quality or beam focusing.

3.7 Numerical aperture

In practical, the value of NA plays a significant role in the application area of PCF-based sensing. NA is inversely proportional to A_{eff}. The NA can be calculated using expression [20].

$$NA = \left(1 + \frac{\pi A_{eff}}{\lambda^2}\right)^{-1/2}. \tag{9}$$

The behavior of the NA is shown in Fig. 9. It is depicted that the NA is centralized with respect to the increment of wavelength. This phenomenon indicates the proposed sensor as an inferior applicant in many optical applications, such as optical coherence tomography (OCT) and medical imaging.

Finally, the suggested sensor for cancerous cell detection shows enhanced relative sensitivity and lower loss with regard to good beam quality. In addition, the monomode characteristic indicates the explored sensor is a promising candidate in the area of cancer-sensing applications. Furthermore, the good response of spot size, NA, and beam quality factors helps to make the superior candidate in differential spectroscopy-based sensing history. As per our knowledge,
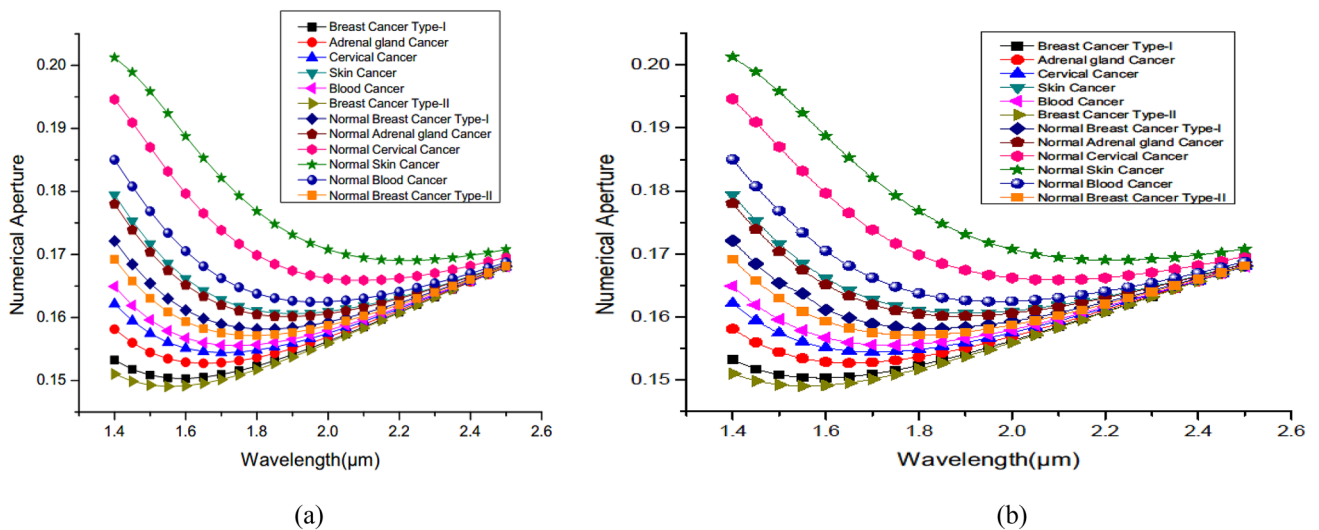

Fig. 9 Numerical aperture vs wavelength for the suggested structure in **a** *X*-polarization and **b** *Y*-polarization

Table 3 List of all variables those are used in the equations

SI	Variable name	Symbol
1	Index of refraction	n
2	Wavelength	λ
3	Relative sensitivity	R_s
4	Index of refraction of the cancerous cell	n_c
5	Real part of the refractive index	$\text{Re}[n_{ei}]$
6	Power ratio	F_p
7	Electric polarized fields	E_x and E_y
8	Magnetic polarized fields	H_x and H_y
9	Confinement loss	L_c
10	Imaginary part of the refractive index	$\text{Im}[n_{eff}]$
11	Effective area	A_{eff}
12	Transverse electric field	$I(r.)$
13	Normalized frequency	V
14	Radius	R
15	Refractive index of core material	n_{co}
16	Refractive index of cladding material	n_{cl}
17	Spot size	W_{eff}
18	Beam divergence angle	θ
19	Numerical aperture	NA

this type of spectroscopy-based sensor is introduced for the first time with enhanced sensitivity (more than 90%) and very low confinement loss.

In the numerical point of view, in Table 3, here are listed all variables name and symbol those are used in different equations. Figures 3, 4, 5, 6, 7, 8 and 9 are illustrated following Eqs. 2–9, respectively. In practical point of view, when the proposed model will be experimentally demonstrated, external factors such as temperature, noise source may change the outcomes compared to simulated results. As a result, the sensitivity response can vary a little but we can assure you that those values will be very close to the suggested outcomes.

4 Conclusion

We present a novel design of a circular lattice cancer cells with enhanced sensitivity and lower confinement loss. The very low confinement loss of 5.3×10^{-9} (dB/m), 4.3×10^{-9} (dB/m), 4.3×10^{-9} (dB/m), 3.6×10^{-8} (dB/m), 6.1×10^{-9} (dB/m), 5.3×10^{-9} (dB/m), and 7.5×10^{-9} (dB/m) are obtained for cervical cancer adrenal gland, skin cancer, blood cancer and breast cancer of type-I and type-II, respectively, with very high relative sensitivities of 94.96%, 95.15%, 94.13%, 94.84%, 95.40%, and 95.51% in X-polarization mode. The calculated performance of overall sensitivity concerning their normal cells is superior to any other previous work. In addition, the monomode characteristics,

good response of spot size, NA, and beam quality factors of the explored sensor make it a prominent candidate for improved differential spectroscopy-based sensing. The proposed design is also easier to fabricate with a lower manufacturing cost by applying modern techniques.

Compliance with ethical standards

Conflict of interest All the authors have read the manuscript and approved this for submission and have no competing interests.

References

1. Ahmed, K., Morshed, M.: Design and numerical analysis of microstructured-core octagonal photonic crystal fiber for sensing applications. Sens. Bio-Sens. Res. **7**, 1–6 (2016)
2. Jabin, M.A., Ahmed, K., Rana, M.J., Paul, B.K., Islam, M., Vigneswaran, D., Uddin, M.S.: Surface plasmon resonance based titanium coated biosensor for cancer cell detection. IEEE Photonics J. **11**(4), 1–10 (2019)
3. Ahmed, K., Ahmed, F., Roy, S., Paul, B.K., Aktar, M.N., Vigneswaran, D., Islam, M.S.: Refractive index-based blood components sensing in terahertz spectrum. IEEE Sens. J. **19**(9), 3368–3375 (2019)
4. Atiqullah, S.M., Palit, A., Reja, M.I., Akhtar, J., Fatema, S., Absar, R.: Detection of harmful food additives using highly sensitive photonic crystal fiber. Sens. Bio-Sens. Res. **23**, 100275 (2019)
5. Ayyanar, N., Raja, G.T., Sharma, M., Kumar, D.S.: Photonic crystal fiber-based refractive index sensor for early detection of cancer. IEEE Sens. J. **18**(17), 7093–7099 (2018)
6. Qin, J., Zhu, B., Du, Y., Han, Z.: Terahertz detection of toxic gas using a photonic crystal fiber. Opt. Fiber Technol. **52**, 101990 (2019)
7. Ramanujam, N.R., Amiri, I.S., Taya, S.A., Olyaee, S., Udaiyakumar, R., Pandian, A.P., Wilson, K.J., Mahalakshmi, P., Yupapin, P.P.: Enhanced sensitivity of cancer cell using one dimensional nanocomposite material coated photonic crystal. Microsyst. Technol. **25**(1), 189–196 (2019)
8. Sharma, P., Sharan, P. and Deshmukh, P.: A photonic crystal sensor for analysis and detection of cancer cells. In: 2015 International conference on pervasive computing (ICPC) (pp. 1–5). IEEE (2015)
9. Sharan, P., Bharadwaj, S.M., Gudagunti, F.D. and Deshmukh, P.: Design and modelling of photonic sensor for cancer cell detection. In: 2014 International conference on the IMpact of E-technology on US (IMPETUS) (pp. 20–24). IEEE (2014).
10. Shirmohammadli, V., Manavizadeh, N.: Numerical modeling of cell trajectory inside a dielectrophoresis microdevice designed

for breast cancer cell screening. IEEE Sens. J. **18**(20), 8215–8222 (2018)

11. Jabin, M.A., Luo, Y., Peng, G.D., Rana, M.J., Ahmed, K., Nguyen, T.K., Paul, B.K., Dhasarathan, V.: Design and fabrication of amoeba faced photonic crystal fiber for biosensing application. Sens. Actuators A **313**, 112204 (2020)

12. Malitson, I.H.: Interspecimen comparison of the refractive index of fused silica. Josa **55**(10), 1205–1209 (1965)

13. Islam, M.S., Sultana, J., Dinovitser, A., Ahmed, K., Ng, B.W.H., Abbott, D.: Sensing of toxic chemicals using polarized photonic crystal fiber in the terahertz regime. Opt. Commun. **426**, 341–347 (2018)

14. Paul, B.K., Ahmed, K., Vigneswaran, D., Sen, S., Islam, M.S.: Quasi photonic crystal fiber for chemical sensing purpose in the terahertz regime: design and analysis. Opt. Quant. Electron. **51**(7), 238 (2019)

15. Islam, M.S., Paul, B.K., Ahmed, K., Asaduzzaman, S., Islam, M.I., Chowdhury, S., Sen, S., Bahar, A.N.: Liquid-infiltrated photonic crystal fiber for sensing purpose: design and analysis. Alex. Eng. J. **57**(3), 1459–1466 (2018)

16. Krishna, G.D., Pillai, V.M., Gopchandran, K.G.: Design of low dispersion and low loss photonic crystal fiber: defected core circular-octagon hybrid lattices. Opt. Fiber Technol. **51**, 17–24 (2019)

17. Kumar, P., Kumar, V., Roy, J.S.: Dodecagonal photonic crystal fibers with negative dispersion and low confinement loss. Optik **144**, 363–369 (2017)

18. Ahmed, K., Paul, B.K., Ahmed, F., Jabin, M.A. & Uddin, M.S.: Numerical demonstration of triangular shaped photonic crystal fibre-based biosensor in the Terahertz range. IET Optoelectron. (2021). https://doi.org/10.1049/ote2.12006

19. Paul, D., Biswas, R., Bhattacharyya, N.S.: Investigating photonic crystal fiber within E to L communication band with different material composites. Optik **126**(23), 4640–4645 (2015)

20. Tsai C., Huang S.: Water distribution in cancer and normal cells. (2012). http://laser.ee.ntu.edu.tw/. Accessed 12 Dec 2020